OTA Measurement for IoT Wireless Device Performance Evaluation: Challenges and Solutions

Penghui Shen, *Student Member, IEEE*, Yihong Qi, *Senior Member, IEEE*, Wei Yu, *Member, IEEE*, Jun Fan, *Fellow, IEEE*, and Fuhai Li, *Member, IEEE*

***Abstract*—The explosion of applications of Internet of Things (IoT) wireless devices urgently requires over-the-air (OTA) performance evaluations. However, the challenges mainly due to the fact that the ubiquitous IoT device applications have made it necessary for OTA measurements to be operated in accurate, fast, and cost-effective ways. This paper proposes a series of solutions for improving the standard OTA measurements to meet the IoT OTA requirements. For single-input single-output (SISO) terminals, three test techniques are introduced for speeding up their total isotropic sensitivity tests and improving the test accuracy. For IoT multi-input multioutput (MIMO) devices, the radiated two-stage (RTS) method is introduced. The detailed theories are described mathematically, including the pattern measurement error elimination and the inverse matrix auto-solving. The advantages of the RTS on MIMO system diagnosis are outlined. Besides, a smart test system was introduced, which is suitable for a general office building. Both SISO and MIMO can be conducted in this chamber, resulting in great cost saving. Thus, with innovations on hardware and methodologies, the OTA evaluations can be accommodated and helpful for the IoT industry.**

***Index Terms*—Internet of Things (IoT), over-the-air (OTA), radiated two-stage (RTS).**

I. Introduction

INTERNET of Things (IoT) devices are estimated to reach 50 billion in year 2020, with a large percentage of the IoT devices being wireless enabled [1], [2]. Wi-Fi, global positioning system, Bluetooth, ZigBee, radio frequency (RF) identification, 2G/3G/4G cellular, and the coming 5G narrow band IoT are popular wireless connecting technologies for IoT [3]–[6]. Wireless connecting reliability, data rate, coverage, connection speed, and security are the figures of merit (FoMs) that have critical impacts on user experience and cost of IoT systems [7]–[10]. The IoT device RF performance plays the most important part in the above mentioned FoMs.

Similar to how measurements and standardizations helped the cellular and telecommunication industry, evaluations of wireless device performance will spur massive amounts of applications and deployments of IoT. The over-the-air (OTA) method is the standard methodology for cellular phone industry organizations such as the Third Generation Partnership Project (3GPP) and the Cellular Telecommunication and Internet Association (CTIA) [11], [12]. OTA test can help to promote IoT industry in three stages. In the research and development (R&D) stage, OTA could help engineers to quantify the RF performance and ensure the wireless devices' performance. The test results are also critical to efficiently detecting the imperfections and improving the designs for wireless system troubleshooting. A higher performance wireless system could cover a wider range, which results a thinner layout of IoT network. In the mass product line stage, the RF performance consistency could be detected for removing the unqualified products to guarantee the reliability of the entire network. And in the certification stage, OTA testing is critical to ensure system performance and compatibility with other systems and environment.

For a single-antenna configured terminal, the uplink FoM is effective isotropic radiated power (EIRP) for directional performance evaluation and total radiated power (TRP) for mobile device or omnidirectional performance evaluation; the downlink FOM is effective isotropic sensitivity (EIS) for directional performance evaluation and total isotropic sensitivity (TIS) for mobile or omnidirectional device performance evaluation [11], [12]. For a multiantenna configured system, the only FoM is throughput for the integrated air-link performance evaluation [13]–[15].

In the R&D process of an IoT RF front end, the antenna and the radio transmitter and receiver are measured and evaluated separately. Generally, EIRP and TRP are depended on the performance of the antenna and the power amplifier (PA) transmitted power. The PA's output power is also related to its load impedance, which is the antenna input impedance; the variation of the antenna impedance can significantly affect the PA output power hence the EIRP and TRP. There exists a similar situation in the downlink performance evaluation, where

Manuscript received May 31, 2018; revised August 9, 2018; accepted September 1, 2018. Date of publication September 4, 2018; date of current version February 25, 2019. This work was supported in part by the Chinese Ministry of Education—China Mobile Research Foundation under Grant MCM 20150101, and in part by the National Natural Science Foundation of China under Grant 61671203. *(Corresponding author: Yihong Qi.)*

P. Shen is with the College of Electric and Information, Hunan University, Changsha 410082, China, and also with General Test Systems, Inc., Shenzhen 518000, China (e-mail: penghui.shen@generaltest.com).

Y. Qi is with the College of Electric and Information, Hunan University, Changsha 410006, China, with General Test Systems, Shenzhen 518102, China, and also with the EMC Laboratory, Missouri University of Science and Technology, Rolla, MO 65409 USA (e-mail: yihong.qi@generaltest.com).

W. Yu is with General Test Systems, Inc., Shenzhen 518000, China (e-mail: fred.yu@generaltest.com).

J. Fan is with the EMC Laboratory, Missouri University of Science and Technology, Rolla, MO 65409 USA (e-mail: jfan@mst.edu).

F. Li is with the College of Electric and Information, Hunan University, Changsha 410082, China (e-mail: fuhai-li@vip.sina.com).

Digital Object Identifier 10.1109/JIOT.2018.2868787

2327-4662 © 2018 IEEE. Personal use is permitted, but republication/redistribution requires IEEE permission.
See http://www.ieee.org/publications_standards/publications/rights/index.html for more information.

Authorized licensed use limited to: HUNAN UNIVERSITY. Downloaded on March 04,2021 at 08:41:10 UTC from IEEE Xplore. Restrictions apply.

the separated measurement of antenna and receiver sensitivity might differ from the integrated RF front end performance evaluation [7], [16], [17]. Practically, due to limited space or cost saving there are no RF connectors in most IoT devices, which makes the OTA measurement the only viable test methodology for IoT uplink and downlink performance evaluations.

A. Challenges of OTA Test for IoT Wireless Devices

There are three types of wireless IoT devices, receive/transmit only devices, single-input single-output (SISO) units, and multi-input multioutput (MIMO) terminals. The OTA measurement accuracy, complexity, and speed need to be carefully investigated for the different types of device to obtain optimized solutions.

OTA needs to be performed in R&D, certification, and mass production stages. The large number of IoT system applications have made it necessary for IoT OTA measurements to be operated in accurate, fast and cost-effective ways. Simply adopting the current OTA standard methods in the CTIA and 3GPP could result in high hardware cost, a long measurement period, and a large measurement uncertainty of ± 2.65 dB for SISO test and an even larger uncertainty for MIMO test [12], [15]. Thus, the major challenges for IoT OTA lie on speed, accuracy, and cost.

1) Challenge in SISO Test Speed: According to the OTA test standards [12]–[15], TIS is accessed through integrating the measured 3-D EIS values. An EIS measurement requires to turn down the air link power step by step until reaching a special communication bit/frame error rate (BER/FER), which is called the power-stepping method [8], [12], [18]. That is quite time-consuming. An accurate BER reading under each fixed air link power needs a large sample space for ensuring accuracy, which expends a long period for EIS, as well as TIS. Taking the global system for mobile communication (GSM) protocol as an example, about 40 min are required for just one TIS measurement based upon the CTIA and 3GPP recommended test configurations and methods, which may seriously degrade the efficiency of R&D and product line.

2) Challenge in SISO Test Accuracy: For TIS measurements, besides the test uncertainties contributed by the power adjusting step and BER sampling space, one more factor may greatly impact the TIS accuracy. An interval of 15° in both phi and theta axes is specified for the spatial sampling measurement of TRP, while an interval of 30° is specified for TIS. This is a balance between TIS test period and accuracy. For most cellular communication terminals, 30° interval is sufficient to fully characterize the device's received performance since the frequency is low (<3 GHz) and the antenna beam is usually wide [9], [19]. However, for the case that the device under test (DUT) antenna beams are novel, such as the high-direct Wi-Fi router working at 5.8 GHz, the interval of 30° may not be able to catch the major lobe [19]. In this condition, the uncertainty could be much larger than the defined ± 2.65 dB [12].

3) Challenge in MIMO Test Accuracy: MIMO OTA measurement is quite different in theory foundations. MIMO is based on spatial diversities in multipath propagations to enable transmission of multistreams [20], [21]. The characteristics of the propagation environments could significantly affect the MIMO throughput. For MIMO OTA measurements, the multipath fading models should be considered [11], [22], [23]. The MIMO test system should set up environments for channel model simulations in chamber. The only CTIA certificated approach is the multiple probe anechoic chamber (MPAC) method, which utilizes an antenna surrounding hardware environment for simulating the multipath fading. The system is extremely difficult for calibrations and operations since of its complex hardware, which also brings many test uncertainties. A proposal showed that for three MPAC systems under the same configurations, the test difference could be up to 7.31 dB [24].

4) Challenge in IoT OTA Test Cost: As there are versatile IoT applications in different business sectors with different business scales, the standard certification test chambers are generally too large to fit in a standard office building. Despite of the chamber's cost, the customer needs a place large enough to hold the test system. And the standard test chambers for SISO and MIMO have different hardware, which means that at least two chambers are required for covering the SISO and MIMO tests [25]–[27].

B. Proposed Solutions

Both test hardware and methodologies are necessary to be innovated for overcoming the mentioned four challenges and help fit the OTA measurement into the IoT industry. A series of solutions is proposed in this paper for carrying the IoT OTA measurement into accurate, fast, and cost-efficient approaches.

1) Test Methodologies for SISO and Receive/Transmit Only Devices: Three types of TIS test methods are introduced for reducing the test period and improving the accuracy. The methods are all based on the fact that TIS could be acquired through combining the receiver sensitivity and the antenna pattern, both of which can be measured separately. The sensitivity is measured via the power-stepping method, which is time-consuming but conducted only once. At any other DUT orientation, just the antenna gain is measured. Basically, we can set a smaller power adjusting step and a larger sample size to improve the sensitivity test accuracy, and with risking only seconds increased on the test period.

The antenna pattern can be achieved through three ways: 1) the received signal strength indication (RSSI)-based technique; 2) the co-frequency-based method; and 3) the BER-shape-based algorithm. First, the antenna pattern can be measured through a few RSSI readings, which are much faster and more accurate than threshold BER/FER searches. Then patterns of receiving and transmitting are the same in shape for transmit-receive co-frequency devices so we can use the TRP pattern for TIS calculation. As a result, the reliability and accuracy of TIS and TRP are comparable. Especially, this method can be perfectly adopted for Wi-Fi SISO OTA, which

Authorized licensed use limited to: HUNAN UNIVERSITY. Downloaded on March 04,2021 at 08:41:10 UTC from IEEE Xplore. Restrictions apply.

means Wi-Fi TIS values can be acquired with a sampling interval of 15° in both phi and theta axes. Third, the BER-downlink power curves at all DUT orientations are invariant in shape, and the offset between any two curves equals the antenna gain difference. Actually, with reducing the sensitivity test uncertainty and decreasing the pattern test period, the TIS test accuracy and speed can be optimized simultaneously for the IoT SISO OTA.

2) Test Methodology for MIMO Devices: For IoT MIMO OTA, the radiated two-stage (RTS) method is introduced, which is same in theory foundations with MPAC, but different in realizations. The channel models are totally calculated on baseband and simulated by software in RTS, which makes RTS a simple and cost-efficient solution for MIMO. The RTS method can be implemented in a SISO chamber. Compared to MPAC, the RTS hardware is much simpler. As a result, less test uncertainties would be brought in. Typically, the repeatability of RTS is within ±0.5 dB [31], [32].

The RTS method was proposed in 2014, and accepted by the 3GPP technical specification (TS) 37.544 in 2018 [7], [18]. Many improvements and changes in theory, procedure, and measurement uncertainty analysis have been proposed for the RTS method standardization [28]–[30]. In this paper, the RTS method is updated in two aspects: 1) the theory foundation and 2) recent progress. First, the complete RTS formulas for MIMO OTA test are presented. Second, two key techniques: 1) the invert matrix auto solving process and 2) the pattern measurement error elimination are proposed, with experiments showing the relationship between the two port isolation values and the throughput measurement uncertainties. Third, the RTS-based MIMO device diagnostic is outlined. Finally, the RTS standardizations in the 3GPP is presented, where the harmonization comparison results between the RTS and the MPAC method are presented. Experiments show that the two methods are quite concordant [31], [32].

The RTS could also be adopted for the coming 5G massive MIMO OTA tests. For the 5G OTA R&D, the progress on the 4G LTE pioneered RTS will help pave the way to the massive MIMO applications on the 5G active antenna system, user equipment (UE), and chipset OTA. The report on the progress of RTS is not going to help the current LTE MIMO measurement, but will cast light for the 5G MIMO OTA.

3) Comprehensive Test System for IoT OTA: This paper also provides a smart SISO OTA test system that is suitable for R&D in an office building. Besides, since the RTS method could be implemented based on a SISO chamber [21]–[30], the IoT SISO and MIMO OTA can be conducted in just one system. Apart from the cost saving on hardware and estate, the comprehensive test system is very convenient for R&D and production line because of its small size.

The rest is arranged as follows: the solutions for the SISO and receive/transmit only IoT devices are organized in Section II with the theories and experiments detailed, followed by the RTS method for IoT MIMO OTA test in Section III with the theories and recent progresses described; in Section IV, the conclusions are listed.

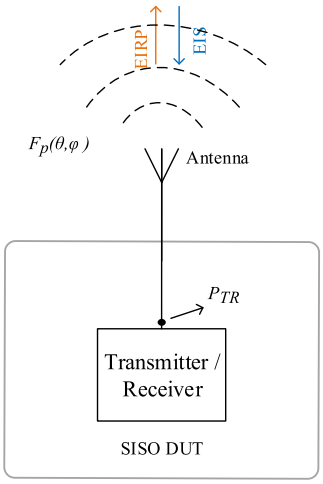

Fig. 1. SISO DUT simplified diagram for EIRP and EIS definition descriptions.

II. OTA Solutions for SISO and Receive/Transmit Only Devices

A. EIRP, TRP, EIS, and TIS Definitions

A single-antenna configured DUT is simplified in Fig. 1, where $F_p(\theta, \varphi)$ represents the antenna gain at angle (θ, φ) in the p polarization (V or H) and P_{TR} is the excited power at the antenna feeding (also the receiver input).

EIRP is the directional power actually radiated by the antenna, which is specified as [12]

$$\mathrm{EIRP}_p(\theta, \varphi) = P_{\mathrm{TR}} * F_p(\theta, \varphi). \tag{1}$$

TRP is the total power actually radiated by the antenna, which is the EIRP-related spherical integration

$$\mathrm{TRP} = \int_{\theta=0}^{\pi} \int_{\varphi=0}^{2\pi} \frac{[\mathrm{EIRP}_H(\theta, \varphi) + \mathrm{EIRP}_V(\theta, \varphi)]\sin(\theta) d\varphi d\theta}{4\pi}. \tag{2}$$

EIS is defined as

$$\mathrm{EIS}_p(\theta, \varphi) = \frac{P_{\mathrm{sen}}}{F_p(\theta, \varphi)} \tag{3}$$

where P_{sen} denotes the radiated sensitivity, which is the received power at receiver input ensuring the DUT operates stably at its threshold BER value [8]. It is an angle-independent factor.

Further, TIS is calculated as

$$\mathrm{TIS} = \frac{4\pi}{\int_{\theta=0}^{\pi} \int_{\varphi=0}^{2\pi} \left[\frac{1}{\mathrm{EIS}_H(\theta,\varphi)} + \frac{1}{\mathrm{EIS}_V(\theta,\varphi)} \right] \sin(\theta) d\varphi d\theta}. \tag{4}$$

TRP measurement is generally fast and accurate since the DUT radiated power is caught and measured via high-precision instruments (such as the power meter) at every orientation. TIS test is always time-consuming based on the standard power-stepping method since the cumbersome process of stable BER threshold (for example, 2.44% for GSM) search is required to be conducted at every DUT orientation and polarization.

Authorized licensed use limited to: HUNAN UNIVERSITY. Downloaded on March 04,2021 at 08:41:10 UTC from IEEE Xplore. Restrictions apply.

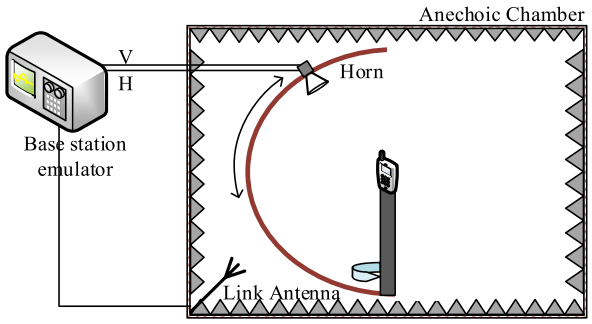

Fig. 2. Typical system for TRP and TIS measurement.

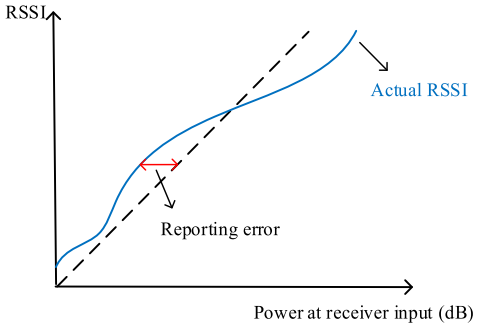

Fig. 3. RSSI reporting errors.

A typical single-antenna configured SISO test system for TRP and TIS is shown in Fig. 2, including a horn antenna (containing V and H polarizations), a turntable, and a link antenna for loop communications. For a certificated chamber, the distance between the quiet zone and the chamber antenna should meet the far-field requirements at all bands [12], so the chamber is usually quite huge. Further, an interval of 15° in both phi and theta axes on the DUT spherical surface is recommended for TRP test, and an interval of 30° is specified for TIS.

Combining (3) and (4), TIS can be expressed as

$$\mathrm{TIS} = \frac{4\pi * P_{\mathrm{sen}}}{\int_{\theta=0}^{\pi}\int_{\varphi=0}^{2\pi}[F_H(\theta,\varphi)+F_V(\theta,\varphi)]\sin(\theta)\ d\varphi d\theta}. \quad (5)$$

It indicates that antenna pattern and sensitivity can measured separately and then combined for TIS calculation, which is the theory foundation of the following three fast methods.

B. RSSI-Based Technique

For the RSSI supported protocols, such as GSM, Wi-Fi, ZigBee, and so on, RF receiver could evaluate the power at the receiver input port (marked in Fig. 1) through an inside digital signal process (DSP) and then report the value to the base station emulator (BSE) OTA. A typical RSSI reporting system has a nonlinear error. As indicated by the schematic in Fig. 3, the x-axis represents the absolute power level at receiver, the y-axis indicates the relative RSSI reading, and the difference between the two lines is the reporting error (in dB format). The errors

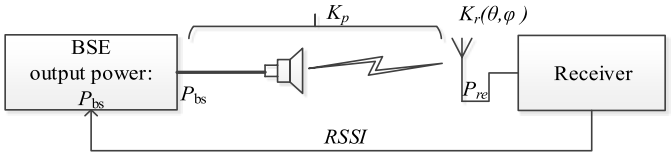

Fig. 4. Simplified system for TIS measurement.

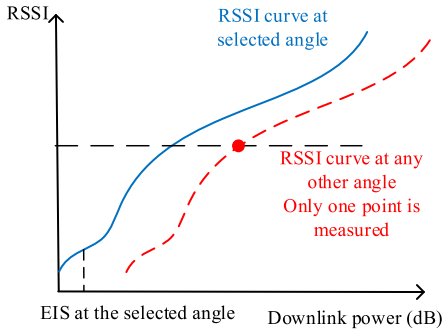

Fig. 5. Measured RSSI-downlink power curve at the selected angle.

should be carefully issued so that the TIS results could not be influenced.

The test system is illustrated in Fig. 2 and simplified in Fig. 4, where P_{bs} is the instrument output power; K_p is the chamber path loss, consisting the chamber antenna gain; $K_r(\theta,\varphi)$ is the DUT antenna gain; and P_{re} is the received power at the DUT antenna feeding and also the receiver input. All formulas and figures in the rest of this section are in dB format by default

$$P_{\mathrm{re}} = P_{\mathrm{bs}} + K_p + K_r(\theta,\varphi) \quad (6)$$

where $P_{\mathrm{bs}} + K_p$ stands for the defined downlink power.

RSSI reporting is the estimation of the power at the receiver

$$\mathrm{RSSI} = f\big(P_{\mathrm{bs}} + K_p + K_r(\theta,\varphi)\big). \quad (7)$$

Thus, for all angles, the RSSI-downlink power curves are the same in shape. The offset between two curves equals to the antenna gain difference. Then, the test procedure is explained as follows.

1) Keep the power P_o fixed and measure the RSSI readings at all DUT angles.
2) Select the maximal RSSI reporting angle and conduct an EIS search through the power-stepping method. Moreover, the RSSI readings are required to be recorded during the power-stepping process. So at the selected angle, besides the EIS value (marked as EIS_s), the RSSI-downlink power curve is plotted, as shown by the real line in Fig. 5.

For any other angle, a single RSSI reading is measured, as shown by the red marker in Fig. 5. The offset on the x-axis between the red marker and the real curve could be easily calculated which is also the antenna gain difference (marked as ΔK_r). Then, the EIS value at this angle is

$$\mathrm{EIS}_r = \mathrm{EIS}_s - \Delta K_r. \quad (8)$$

Actually, only one EIS search process and a few RSSI readings are required for a TIS measurement. Besides, no reporting

Authorized licensed use limited to: HUNAN UNIVERSITY. Downloaded on March 04,2021 at 08:41:10 UTC from IEEE Xplore. Restrictions apply.

errors are introduced since no RSSI values are included in the final EIS and TIS calculations.

C. Co-Frequency-Based Method

For transmit-receive co-frequency devices, the patterns of receiving and transmitting are the same, which is clear from (1) and (3). The TIS test procedure depends on two steps: 1) measuring the EIS value at a random angle with the power stepping method and 2) carrying out a complete TRP test. From the TRP pattern (also the TIS pattern) and the single EIS, the EIS values at other orientations could be achieved, as well as the TIS. As discussed before, TRP test is much more accurate and faster than TIS. So this approach makes the TIS test accuracy and speed comparative to TRP.

D. BER Curve-Based Method

BER is closely related to the received power at receiver input front. Anderson *et al.* [17] provided the BER function derivation based on Gaussian minimum shift keying modulation over a nonloss additive white Gaussian noise channel, as (in real)

$$\mathrm{BER} = \frac{1}{2}\mathrm{erfc}\left(\sqrt{\frac{P_{\mathrm{re}}}{T * Q}}\right) = g(P_{\mathrm{re}}) \tag{9}$$

where P_{re} is the received power, and Q and T are the bit rate and the white noise power spectral density, respectively.

According to the test system in Fig. 4, the BER function could be further rewritten as

$$\mathrm{BER} = g\big(P_{\mathrm{re}} + K_p + K_r(\theta, \varphi)\big). \tag{10}$$

Similar to the RSSI-based method, the BER-downlink power curves are same in shape and the offsets are the corresponding antenna gain differences. So the antenna pattern can be obtained through the following two steps. First, measure an EIS through the power-stepping method and record the BER-power curve at a random angle, as the real line in Fig. 6. Second, at any other angle, once a BER reading between 0% and 100% is acquired (as the red marker in Fig. 6), the antenna gain difference would be calculated, as well as the corresponding EIS value. This approach is much faster than the special BER threshold search process, since much less BER search steps are needed.

It is worth indicating that by utilizing the three measurement algorithms, only one sensitivity search is required for TIS test where the power-stepping process is adopted. So we can use a smaller step and a larger sampling size than the standard definition for improving the sensitivity search accuracy, and with risking only seconds increased on the measurement period. That is also the advantage of the three methods.

E. Comparisons

For the TIS measurement period and accuracy validations, a multiple probe configured SISO anechoic chamber is used in this paper, as shown in Fig. 7. The eleven measurement antennas are located asymmetrically, with an interval of 15°

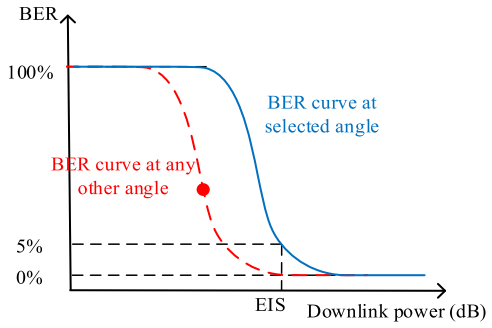

Fig. 6. BER-downlink power curves at two DUT angles.

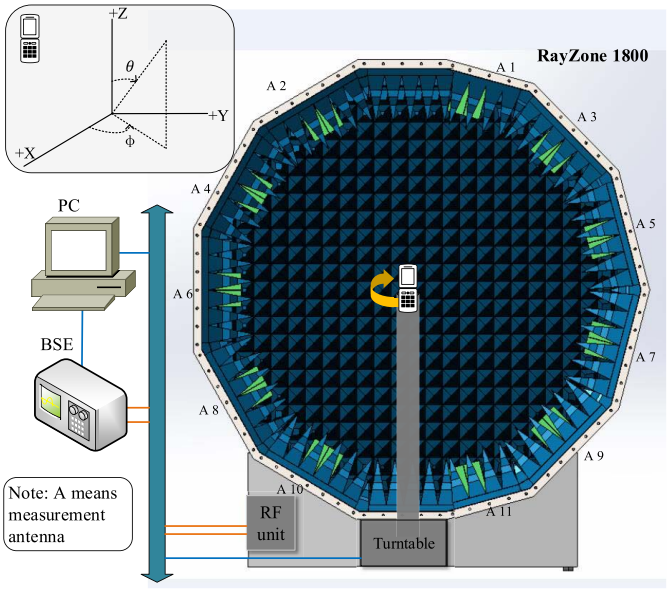

Fig. 7. RSSI reporting errors.

in the theta-axis, for meeting the CTIA standard TRP and TIS 3-D test requirements [7]–[10]. Specially, the chamber size is about 1.9 m × 1.8 m × 1.2 m, that is much smaller than the certified chamber and suitable for office buildings [33].

The validations are carried out in three groups.

1) The RSSI-based method versus the power-stepping method on LTE protocol.
2) The co-frequency-based method versus the power-stepping method on Wi-Fi protocol.
3) The BER curve-based method versus the power-stepping method on GSM protocol.

All the test set-ups are listed in Table I. Two things are emphasized: first, the EIS search configurations and process (including the power adjustment step, the sampling size, the BSE initial output power, etc.) in all validations are the same, so that the measurement periods would not be influenced by any factors except the test methods and second, during the measurements, the DUT is fixed and all hardware configurations are invariant, including the positions, connections, the BSE, the DUT location, the environment temperature ($18 \pm 1°$), etc.

Authorized licensed use limited to: HUNAN UNIVERSITY. Downloaded on March 04,2021 at 08:41:10 UTC from IEEE Xplore. Restrictions apply.

TABLE I
MEASUREMENT PARAMETERS

Parameters	Value
Instruments	PC, R&S CMW500
Anechoic chamber	RayZone 1800 from General Test Systems Inc. in Shenzhen [33].
Test frequency	2110 MHz for LTE 2472 MHz for Wi-Fi 960 MHz for GSM
Power adjustment step for sensitivity search	0.2 dB
Sampling size	> 20000 bits (or > 4000 frames)

TABLE II
COMPARISONS

Protocol	Method	TIS (dBm)	Diff. (dB)	Period (mins)	Times
LTE	power-stepping	-96.10	0.30	20	4
	BER curve-based	-96.40		5	
Wi-Fi	power-stepping	-80.31	0.89	88	8.8
	co-frequency	-81.20		10	
GSM	power-stepping	-107.00	0.63	60	12
	RSS-based	-107.63		5	

The test results and periods are shown in Table II. In short, by utilizing the presented three algorithms, the test speed can be decreased by more than 8.8 times on Wi-Fi and GSM protocols. The TIS differences are within 1 dB, which may be mainly caused by the DUT itself (the DUT temperature and stability). The SISO TIS measurement uncertainty analysis are detailed in [7], [8], [10], and [12].

III. RTS METHOD FOR MIMO DEVICES

For IoT MIMO OTA measurement, the RTS technique is updated in this section, with the theory foundations proposed in Section III-A, followed by the inverse matrix solving method in Section III-B; in Section III-C, the reporting error elimination technique is presented; the RTS-based composition method for R&D is described in Section III-D, and then the recent progress is provided in Section III-E.

A. Theory of the RTS Method

MIMO OTA measurement should be conducted with fading channel being considered. Channel models are used to characterize the typical complex propagation environments of MIMO DUT applications, including information about the arrival angles at UE, the departure angles at base station, the path-loss, the delay, the power distribution, the Doppler influence, the cross-polarization rate, etc., as shown in Fig. 8.

Theoretically, for a $S \times U$ MIMO system (S is transmit antennas and U is receive antennas), the transmitting signals for the BSE [marked as $x(t)$] to the receiver inputs [marked as $y(t)$] could be described as

$$y(t) = H(t) * x(t) \tag{11}$$

where $H(t)$ is a channel coefficient matrix, containing all information of propagations from the BSE to MIMO receivers.

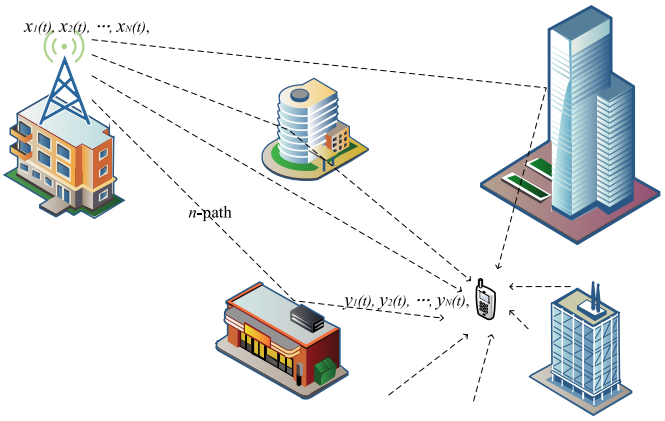

Fig. 8. MIMO complex propagation environment diagram.

The (u, s) element ($u = 1, 2, \ldots, U$; $s = 1, 2, \ldots, S$) of $H(t)$ marked as $h_{u,s}(t)$, representing the signals from sth transmitter to uth receiver input, can be written as

$$h_{u,s}(t) = \sum_{n=1}^{N} h_{n,u,s}(t) \tag{12}$$

where $h_{n,u,s}(t)$ is the vector crossing the nth path and N is the number of arrival paths defined in channel model.

Additionally, based on the 3-D channel model proposed in [34], $h_{n,u,s}(t)$ is elaborated as

$$\begin{aligned} h_{n,u,s}(t) = \sum_{m=1}^{M} & e^{-j2\pi\lambda^{-1}D_s^{tx}(\Omega_m^{tx})} * e^{-j2\pi\lambda^{-1}D_u^{rx}(\Omega_n^{rx})} * e^{-jk\mathbf{v}t} \\ & * \begin{bmatrix} F_u^{rx(V)}(\Omega_n^{rx}) \\ F_u^{rx(H)}(\Omega_n^{rx}) \end{bmatrix}^T \cdot \begin{bmatrix} \chi_{n,m}^{V,V} & \chi_{n,m}^{V,H} \\ \chi_{n,m}^{H,V} & \chi_{n,m}^{H,H} \end{bmatrix} \\ & \cdot \begin{bmatrix} F_s^{tx(V)}(\Omega_m^{tx}) \\ F_s^{tx(H)}(\Omega_m^{tx}) \end{bmatrix} \end{aligned} \tag{13}$$

where $F_s^{tx(V)}$ and $F_s^{tx(H)}$ are the sth transmitting antenna gains; $\chi_{n,m}^{V,V}$, $\chi_{n,m}^{V,H}$, $\chi_{n,m}^{H,V}$, and $\chi_{n,m}^{H,H}$ are the complex path loss factors; $F_u^{rx(V)}$ and $F_u^{rx(H)}$ are the uth receiving antenna gains; Ω_m^{tx} and Ω_n^{rx} are the angle of department and arrival separately; $D_s^{tx}(\Omega_m^{tx})$ and $D_u^{rx}(\Omega_n^{rx})$ are the phases of department and arrival, respectively; λ is the wavelength; and $k\mathbf{v}$ denotes the Doppler frequency influence [34].

We can simplify (13) as

$$h_{n,u,s}(t) = \begin{bmatrix} F_u^{rx(V)}(\Omega_n^{rx}) \\ F_u^{rx(H)}(\Omega_n^{rx}) \end{bmatrix}^T \cdot \Theta_{n,u,s}. \tag{14}$$

Combining (12) and (14), (11) can be rewritten as

$$\begin{aligned} y(t) = \sum_{n=1}^{N} & \begin{bmatrix} \begin{bmatrix} F_1^{rx(V)}(\Omega_n^{rx}) \\ F_1^{rx(H)}(\Omega_n^{rx}) \end{bmatrix}^T \cdot \Theta_{n,1,1} & \cdots & \begin{bmatrix} F_1^{rx(V)}(\Omega_n^{rx}) \\ F_1^{rx(H)}(\Omega_n^{rx}) \end{bmatrix}^T \cdot \Theta_{n,1,S} \\ \vdots & \ddots & \vdots \\ \begin{bmatrix} F_S^{rx(V)}(\Omega_n^{rx}) \\ F_S^{rx(H)}(\Omega_n^{rx}) \end{bmatrix}^T \cdot \Theta_{n,U,1} & \cdots & \begin{bmatrix} F_S^{rx(V)}(\Omega_n^{rx}) \\ F_S^{rx(H)}(\Omega_n^{rx}) \end{bmatrix}^T \cdot \Theta_{n,U,S} \end{bmatrix} \\ & * x(t). \end{aligned} \tag{15}$$

Authorized licensed use limited to: HUNAN UNIVERSITY. Downloaded on March 04,2021 at 08:41:10 UTC from IEEE Xplore. Restrictions apply.

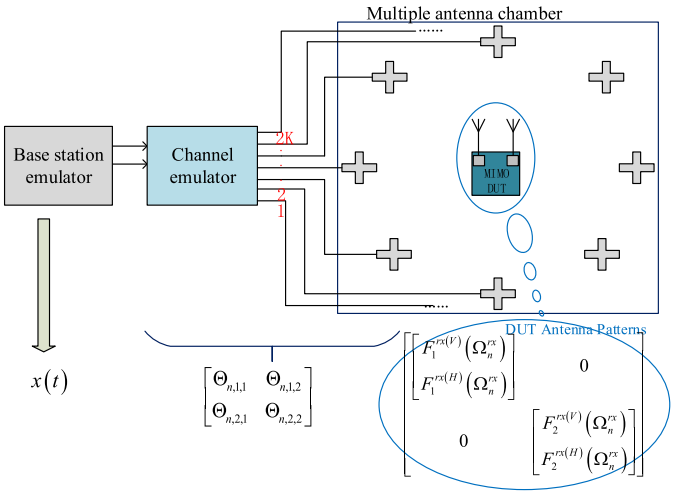

Fig. 9. MPAC measurement system diagram.

Further, the received vector $y(t)$ is expressed as

$$y(t) = \left(\sum_{n=1}^{N} \begin{bmatrix} \begin{bmatrix} F_1^{rx(V)}(\Omega_n^{rx}) \\ F_1^{rx(H)}(\Omega_n^{rx}) \end{bmatrix}^T & \cdots & 0 \\ \vdots & \ddots & \vdots \\ 0 & \cdots & \begin{bmatrix} F_S^{rx(V)}(\Omega_n^{rx}) \\ F_S^{rx(H)}(\Omega_n^{rx}) \end{bmatrix}^T \end{bmatrix} \cdot \begin{bmatrix} \Theta_{n,1,1} & \cdots & \Theta_{n,1,S} \\ \vdots & \ddots & \vdots \\ \Theta_{n,U,1} & \cdots & \Theta_{n,U,S} \end{bmatrix} \right) * x(t). \quad (16)$$

Equations (11)–(16) are the theory foundations of MIMO OTA measurements. In this paper, 2 × 2 MIMO is used as an example to explain the implements for convenience. The MPAC method uses the antenna-surrounding hardware plus the channel emulator to simulate the complex multipath environment. Fig. 9 indicates the MPAC system, where K dual-polarization measurement antennas are used for simulating the channel models physically. Each polarization corresponds to a channel emulator output. The received vectors are the integration of DUT antenna patterns and the propagation surroundings, as detailed in (16). The MPAC method is challenged for three points. First, the complex hardware would lead to a very high cost, and a large place is required for holding. Then, it is extremely difficult for calibrations and operations, since all antennas need to be calibrated carefully for ensuring test accuracy. Third, the MPAC method can hardly support the 3-D channel model simulations.

A conducted two-stage (CTS) method was introduced in [11], which is based on the fact that the signal $y(t)$ can be calculated through integrating the channel model and the DUT antenna patterns, and then fed into the DUT receiver inputs directly, as illustrated in Fig. 10 where the signals are delivered into the receivers directly via two real RF

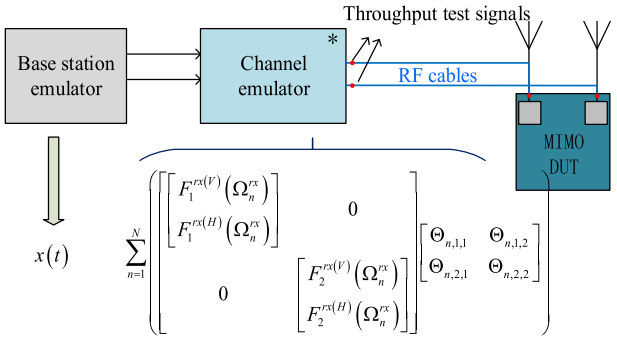

Fig. 10. In the CTS method, the throughput test signals are fed into the receivers via RF cables.

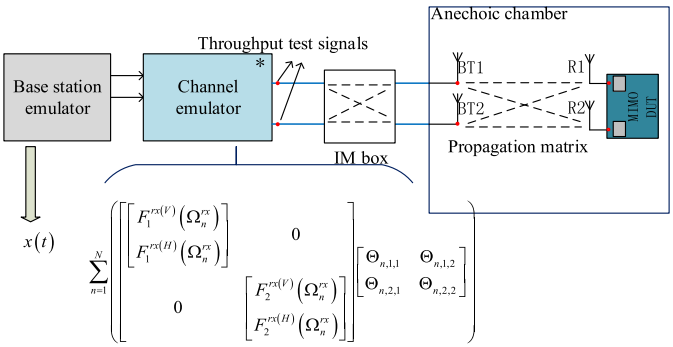

Fig. 11. In the RTS method, the throughput test signals are fed into the receivers in a radiated approach.

cables, respectively (without cross-talking). In the rest of this paper, $y(t)$ is recorded as the throughput test vector for convenience. However, besides the inconvenient RF connectors, the CTS method was challenged since the self-interference (mainly caused by the DUT digital circuits, RF modules, and power blocks) cannot be considered during testing. The self-interference could be coupled via DUT antennas and fed into the RF receivers, which finally causes significant desensitization and greatly affects the throughput results [18]–[21]. The CTS test result cannot reflect the DUT's real wireless performance.

For solving these issues, the RTS was proposed in [21], where the throughput test signals were delivered into the MIMO receivers through a radiated approach. Fig. 11 shows the schematic of a RTS test system, the DUT is held in a chamber, and a 2×2 RF matrix box is added between the emulator outputs and the measurement antennas for two considerations: first, the throughput test signals generated by the channel emulator should be sent into the DUT receiver inputs without crosstalk and second, in an anechoic chamber the signal excited at any measurement antenna can be caught by both DUT received circuits and cross propagation environment can be described as a 2×2 matrix (named as the propagation matrix for convenience). The 2×2 matrix box is used for generating the inverse of the propagation matrix so that the emulator simulated throughput test signals are delivered in the receiver inputs without crosstalk, similar to the CTS method.

The self-interference could be contained in the RTS test since the DUT operates at its normal integrated mode during

Authorized licensed use limited to: HUNAN UNIVERSITY. Downloaded on March 04,2021 at 08:41:10 UTC from IEEE Xplore. Restrictions apply.

the whole measurement period, without intrusive connections. Hence, the test results could reflect the DUT true end user experience. The complex channel models are calculated and simulated in instruments, which is much more stable and accurate than the MPAC approach. Additionally, the RTS method can be implemented on SISO chamber hardware, which is much more cost-efficient and affordable.

The RTS test is carried out based on the following three steps. First, conduct the DUT antenna pattern measurement. Second, solve the inverse matrix. Third, measure the MIMO throughput results. The RTS system is shown in Fig. 7. At the second and third stages of the RTS test procedure, just two chamber antennas are selected for the throughput signals transmitting.

B. Inverse Matrix Auto Solving Method

Throughput test signal calculations are presented in Section III-A, and the signals are required to be delivered into DUT receivers OTA and without cross-talking. This is also the reason why the inverse of the propagation matrix is applied. However, there remains two challenges in the inverse matrix solving process, which greatly affect the RTS measurement procedure and accuracy.

1) Challenge 1: As discussed in Fig. 11, the propagation matrix includes the information about the power path losses and the phase offsets form the chamber antenna feedings to the UE RF receiver inputs. We can express the propagation matrix as

$$P = \begin{bmatrix} p_{11}e^{j\varphi_{11}} & p_{12}e^{j\varphi_{12}} \\ p_{21}e^{j\varphi_{21}} & p_{22}e^{j\varphi_{22}} \end{bmatrix} \tag{17}$$

where φ_{ij} and p_{ij} are the phase difference and the path loss from the jth antenna feeding to the ith receiver, respectively.

Since the RTS test is implemented OTA (without intrusive RF cables connected on the DUT), the absolute phase offsets between the antennas and the receivers cannot be obtained. As a result, the elements φ_{ij} in propagation P are unable to be achieved. Therefore, how to solve the inverse matrix of a fixed P is an issue.

2) Challenge 2: The propagation matrix is determined by the factors as the measurement antenna complex gains, the free space in chamber, the DUT antenna complex gains, the DUT orientation, etc. [28], [29]. Each combination of DUT orientation and chamber antennas generates one propagation matrix. It is required to select one combination to do inverse matrix solving and throughput measuring. One basic condition for the inverse calculation is that the propagation matrix is nonsingular. In practice, another factor is required to be considered in the RTS implement.

In the RTS approach, the throughput test signals are sent to the DUT receivers after processing in the inverse matrix and the propagation matrix, as shown in Fig. 11. This transmitting scenario is simplified in Fig. 12, where R_x and T_x mean the receiver input and the emulator output separately, M_{ij} is the (i, j) element of the inverse matrix M, and P_{ij} is the (i, j) component of the propagation matrix P. Then, the signal from T_1 to the two receivers are

$$R_1 = (M_{11} * P_{11} + M_{21} * P_{12}) * T_1$$

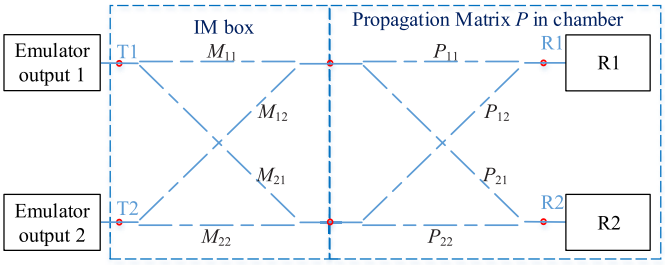

Fig. 12. Schematic of the propagation matrix and the inverse matrix.

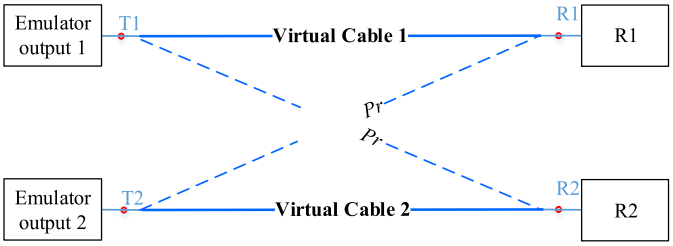

Fig. 13. With the inverse of the propagation matrix applied, the transmitting ports could reach the receivers directly, similar to the conducted working mode.

$$R_2 = (M_{11} * P_{21} + M_{21} * P_{22}) * T_1. \tag{18}$$

Mathematically, we can have $M_{11} * P_{21} + M_{21} * P_{22} = 0$ since M is the inverse of P, which indicates that the received power at the second receiver from the first emulator output is zero. However, there is always remaining power from transmitting port 1 to receiver 2 (mainly caused by reflections, bandwidth, coupling, calculation errors, etc.), which can be accounted as a constant power level for fixed measurement set-ups, and marked as P_r in this paper. The practical application is shown in Fig. 13, where the link from T_x to R_x can be considered as a "virtual cable x," and P_r represents the crosstalk.

Theoretically, we can have $M_{11} * P_{11} + M_{21} * P_{12} = 1$. However, in fact, a real RF circuit has an upper limited gain, which means that the maximal amplitude of the element in the inverse matrix M is limited. In this paper, we assumed that the gain limitation is 1 (in real). The maximal amplitude of the component in M should be no larger than 1. Then, the relationship between the real applied inverse matrix M' and the theoretical one is

$$M' = \frac{1}{A} * M \tag{19}$$

where A is the normalization factor to ensure that the maximal amplitude in M' is 1.

From (18) and (19), in practice applications, we can have

$$P{\cdot}M' = \begin{bmatrix} \frac{1}{A} & P_r \\ P_r & \frac{1}{A} \end{bmatrix}. \tag{20}$$

So with the matrix M' applied, the isolations of the virtual cables are

$$\text{Iso}_1 = \text{Iso}_2 = \frac{1}{A * P_r}. \tag{21}$$

Authorized licensed use limited to: HUNAN UNIVERSITY. Downloaded on March 04,2021 at 08:41:10 UTC from IEEE Xplore. Restrictions apply.

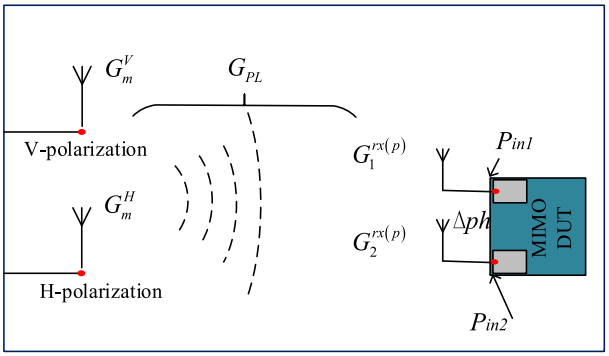

Fig. 14. DUT antenna patterns achievement setups.

The isolation may affect the received signal at the receiver directly and further degrade the sensitivity. The impact depends on the value of the isolation. Experiments in [27] showed the virtual cables' isolations should be larger than 16 dB so that the RTS measurement uncertainties contributed by the remanding cross talking P_r can be negligible, which will be discussed in the rest of this paper. More importantly, it is better to achieve isolation values as large as possible to improve the RTS test reliability and stability. Thus, the second challenge for the inverse matrix calculating process is how to find an appropriate propagation matrix P so that with the corresponding inverse matrix loaded, the isolations of the virtual cables can meet the requirements.

For 2×2 RTS MIMO OTA test, an inverse matrix auto solving algorism was developed in [28], where the two issues were resolved properly with a series of test steps. But for the $M \times M$ ($M > 2$) RTS MIMO OTA test, the two mentioned challenges are still remained. This paper proposes a mathematic technique for overcoming the two challenges, which is much more efficient than the algorism in [28]. And the technique is suitable for handling the $N \times N$ ($N >= 2$) RTS measurement.

3) Solution for the Second Challenge: The technique proposed in this part aims to find the special combination which corresponds to the largest isolation of the virtual cable, and then solve the inverse. For solving the issue, the MIMO DUT patterns are needed. Fig. 14 shows the DUT antenna patterns achievement set-ups, where two cross-polarization antennas were used for antenna patterns measurement and for the 2×2 MIMO throughput test. The MIMO DUT complex antenna pattern at one DUT angle includes the information about the DUT antenna gains of all antennas in both polarizations and the phase differences of received vectors between any two receiver inputs for each measurement antenna, as shown in Fig. 14, where G_m^p is the measurement antenna gain in polarization p, G_{PL} is the chamber path loss, $G_i^{rx(p)}$ is the ith DUT antenna gain in polarization p, P_{in1} and P_{in2} are the received power levels at two receiver inputs, and Δph is the phase difference between the two receivers.

From the measured DUT antenna patterns, for p-polarization measurement antenna, two factors are known.

1) The total power loss from the measurement antenna feeding to the ith receiver input: $G_m^p * G_{\mathrm{PL}} * G_i^{rx(p)}$.
2) The difference between the phase offsets from the same measurement antenna to the two receiver inputs (read from the antenna patterns directly). Especially, α and β are used to represent the phase offsets from the V- and H-polarization measurement antenna to the two receivers separately.

Furthermore, the propagation matrix in Fig. 14 can be rewritten as

$$P = \begin{bmatrix} G_{\mathrm{PL}} * G_m^V * G_1^{rx(V)} * e^{j\varphi_{1V}} & G_{\mathrm{PL}} * G_m^H * G_1^{rx(H)} * e^{j\varphi_{1H}} \\ G_{\mathrm{PL}} * G_m^V * G_2^{rx(V)} * e^{j\varphi_{2V}} & G_{\mathrm{PL}} * G_m^H * G_2^{rx(H)} * e^{j\varphi_{2H}} \end{bmatrix} \tag{22}$$

where only the factors φ_{ij} are unknown.

As sated before, from the antenna patterns, we can have

$$\begin{aligned} \alpha &= \varphi_{2V} - \varphi_{1V} \\ \beta &= \varphi_{2H} - \varphi_{1H}. \end{aligned} \tag{23}$$

Substituting (23) into (22), the propagation matrix can be further rewritten as

$$P = \begin{bmatrix} G_{\mathrm{PL}} * G_m^V * G_1^{rx(V)} & G_{\mathrm{PL}} * G_m^H * G_1^{rx(H)} \\ G_{\mathrm{PL}} * G_m^V * G_2^{rx(V)} * e^{j\alpha} & G_{\mathrm{PL}} * G_m^H * G_2^{rx(H)} * e^{j\beta} \end{bmatrix} \times \begin{bmatrix} e^{j\varphi_{1V}} & 0 \\ 0 & e^{j\varphi_{1H}} \end{bmatrix}. \tag{24}$$

Assume that

$$P_B = \begin{bmatrix} G_{\mathrm{PL}} * G_m^V * G_1^{rx(V)} & G_{\mathrm{PL}} * G_m^H * G_1^{rx(H)} \\ G_{\mathrm{PL}} * G_m^V * G_2^{rx(V)} * e^{j\alpha} & G_{\mathrm{PL}} * G_m^H * G_2^{rx(H)} * e^{j\beta} \end{bmatrix}$$
$$P_H = \begin{bmatrix} e^{j\varphi_{1V}} & 0 \\ 0 & e^{j\varphi_{1H}} \end{bmatrix} \tag{25}$$

where P_B is a known matrix since the measurement antenna gains and chamber free space path loss are known from calibrations, the receiver antenna gains and relative phases α, β are known from measured antenna patterns; P_H is unknown.

From (24) and (25), the theoretical inverse matrix M of propagation matrix P is

$$M = P^{-1} = {P_H}^{-1} \cdot {P_B}^{-1}. \tag{26}$$

It is worth mentioning that ${P_H}^{-1}$ is a diagonal matrix and the amplitudes of all the components are 1. Therefore, we can have

$$|M_{ij}| = |P_{Bij}| \tag{27}$$

where $|P_{Bij}|$ is the amplitude of the (i, j) component in matrix P_B and $|M_{ij}|$ is the amplitude of the (i, j) component in matrix M.

The matrix P_B is known, as discussed in (25). Thus, the amplitude values of all the components in matrix M are known, as shown in (27), as well as the normalization number A. With the factor A obtained, the isolations in (21) can be calculated since P_r is a constant parameter for fixed measurement configurations.

In short, each combination of DUT orientation and chamber antennas generates one propagation matrix. For any propagation matrix, the virtual cables' isolations can be calculated

Authorized licensed use limited to: HUNAN UNIVERSITY. Downloaded on March 04,2021 at 08:41:10 UTC from IEEE Xplore. Restrictions apply.

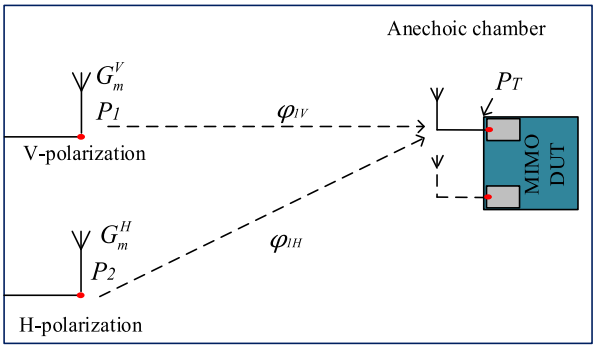

Fig. 15. Measurement set-ups for solving the inverse matrix.

just according to the measured DUT antenna patterns in the first step of the RTS test procedure. Therefore, we can select a suitable combination for inverse matrix solving to meet the isolation requirements. Generally, the combination corresponding to the maximal isolation is selected. So the second challenge is addressed through calculations in this part.

4) Solution for the First Issue: While the special combination was selected in the last part, the propagation matrix is shown in (24), where only the absolute phase offsets from the two measurement antennas to the first receiver (φ_{1V} and φ_{1H}) are unattainable. In this part, the solution to solve the matrix P was presented, where only one small measurement step is required. The test set-ups are simplified in Fig. 15, the hardware is unchanged compared with Fig. 14. The test procedure is detailed as below.

Excite the two selected antenna feedings with two vectors, P_1 and P_2, as shown in Fig. 15. Then, obtain the received power at the first receiver input through RSSI reporting in OTA mode (marked as P_T). We can have

$$|P_1| * |P_2| * \cos(\varphi_{1H} - \varphi_{1V}) = |P_T|. \tag{28}$$

Thus, the phase difference between φ_{1V} and φ_{1H} is calculated and marked as δ

$$\varphi_{1H} - \varphi_{1V} = \delta. \tag{29}$$

Combining (29) and (24), the propagation matrix P becomes

$$P = \begin{bmatrix} G_{\mathrm{PL}} * G_m^V * G_1^{rx(V)} & G_{\mathrm{PL}} * G_m^H * G_1^{rx(H)} * e^{j\delta} \\ G_{\mathrm{PL}} * G_m^V * G_2^{rx(V)} * e^{j\alpha} & G_{\mathrm{PL}} * G_m^H * G_2^{rx(H)} * e^{j(\beta+\delta)} \end{bmatrix} \times e^{j\varphi_{1V}}. \tag{30}$$

Define that

$$P'' = \begin{bmatrix} G_{\mathrm{PL}} * G_m^V * G_1^{rx(V)} & G_{\mathrm{PL}} * G_m^H * G_1^{rx(H)} * e^{j\delta} \\ G_{\mathrm{PL}} * G_m^V * G_2^{rx(V)} * e^{j\alpha} & G_{\mathrm{PL}} * G_m^H * G_2^{rx(H)} * e^{j(\beta+\delta)} \end{bmatrix} \tag{31}$$

where all components are known as discussed before.

From (30) and (31), the inverse matrix of the propagation matrix P is

$$P^{-1} = e^{-j\varphi_{1V}} * P''^{-1}. \tag{32}$$

Formula (32) indicates that after conducting one measurement step, the inverse of the propagation matrix P reminds only one unknown factor φ_{1V}. Further, it is easy to have

$$P''^{-1} \cdot P = \begin{bmatrix} 1 & 0 \\ 0 & 1 \end{bmatrix} * e^{j\varphi_{1V}}. \tag{33}$$

Formula (33) is the key equation for inverse matrix solving for a fixed propagation matrix. It is worth noting that according to (33), with the matrix P''^{-1} applied into the IM box (shown in Fig. 12), we can have the virtual cables as illustrated in Fig. 13. Although the absolute phase offsets of the two "cables" equal to φ_{1V}, which is unable to achieve, the two cables in Fig. 13 are balanced in power loss and phase offset, just like the real cables do. In other words, with applying the matrix P''^{-1}, the emulator outputs are linked to the receiver inputs through virtual cables, respectively. Hence, the absolute phase offsets of the virtual cables are insignificant.

Finally, the real applied inverse matrix should be normalized because of the RF circuit gain limitation

$$M' = \frac{P''^{-1}}{\max\left(\left|P''^{-1}{}_{ij}\right|\right)}, \tag{34}$$

where $|P''^{-1}{}_{ij}|$ is the amplitude of the (i, j) component in matrix P''^{-1}. All factors in P''^{-1} are known as stated before, so that the real applied inverse matrix M' can be calculated.

In summary, from Sections III-B3 and III-B4, for 2×2 RTS test, just one step is required for the inverse matrix solving. Actually, by using the algorithm proposed in this part, only seconds are needed for the entire process of the appropriate combination searching and the inverse matrix solving, which significantly reduces the RTS measurement period and optimizes the RTS test procedure.

Moreover, all the derivations in this section are based on the matrix operation rules. So although the 2×2 MIMO measurement is taken as an example, the algorithm is suitable for $N \times N$ ($N >= 2$) inverse matrix auto solving in the RTS test procedure as well.

5) Throughput Measurement Uncertainties Contributed by the Virtual Cable Isolations: The impact on throughput brought by the virtual cables has been investigated in [30] and [36]. Special designed experiments were carried out to find out the RTS test uncertainty contributed by the degraded isolation. Experiments showed that even in the worst case proposed in [30] (the correlation number of the channel coefficient matrix is up to 0.97), the throughput sensitivity test repeatability is within ± 0.3 dB in the condition that the isolations are greater than 16 dB. Thus, the throughput impact of isolation can be negligible with the isolation larger than 16 dB.

C. Reporting Error Elimination Method

The first step in the RTS test procedure is conducting the antenna pattern measurement in an anechoic chamber. With the aim of measuring the antenna patterns nonintrusively, the DUT chipset needs to support received signal and relative phase (RSRP) reporting. Similar to how the RSSI reporting works in SISO system, the RSRP reporting could report the signal strength at each receiver input and the phase differences

Authorized licensed use limited to: HUNAN UNIVERSITY. Downloaded on March 04,2021 at 08:41:10 UTC from IEEE Xplore. Restrictions apply.

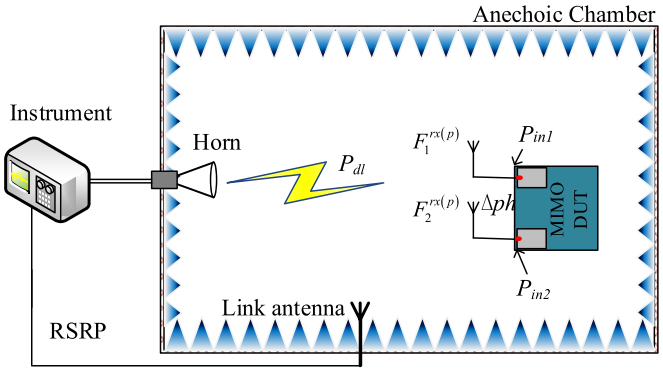

Fig. 16. Simplified block diagram for MIMO DUT antenna patterns achievement in the RTS first stage.

of received signals between any two receivers to the base station OTA. As shown in Fig. 14, for a 2×2 MIMO device, the power at the both receivers P_{in1} and P_{in2} and the received signal phase difference Δph can be estimated by the DUT inside DSP and then reported in OTA mode.

The obtained antenna patterns are loaded into the emulator for throughput measurement signal calculations. However, a general RSRP reporting system has calculating errors for the power and relative phase evaluations, which may be larger than ± 2 dB for power estimation and $\pm 10°$ for phase estimation. More importantly, the RSRP reporting errors are unknown and unavailable in radiated test set-ups. And the power evaluation errors at different receiver inputs may differ, resulting in more difficulties for reporting error analysis. The errors are led into the MIMO DUT antenna pattern measurement results and brought in the throughput test signals which are the integrations of the measured antenna patterns and the selected channel models. The errors may seriously influence the final throughput test accuracy. Thus, an additional challenge for RTS method is how to eliminate the RSRP reporting errors and maintain the test accuracy.

1) RSRP Reporting Errors Description: The 2×2 RTS test system is shown in Fig. 16, which is also SISO measurement supported, where P_{dl} is the total downlink power; $F_j^{rx(p)}$ is the jth DUT antenna gain on p polarization; $P_{\text{in}j}$ is the real actual power value at the jth receiver; and Δph is the real actual phase offset. It is noteworthy that P_{in1}, P_{in2} and Δph are unknown and only the corresponding estimations can be read from RSRP, including errors certainly, as

$$\begin{aligned} P_{\text{in1}} &= R|P_1 * E_1 \\ P_{\text{in2}} &= R|P_2 * E_2 \\ \Delta\text{ph} &= R|\Delta\text{ph} + \psi \end{aligned} \tag{35}$$

where $R|P_j$ and $R|\Delta$ph are the estimations of $P_{\text{in}j}$ and $R|\Delta$ph in reporting, and E_j and ψ are the amplitude and phase reporting errors, separately. Then the measured antenna gains (marked as $R|F_j^{rx(p)}$) and phase shift ($R|\Delta$ph) are achieved as

$$\begin{aligned} R|F_1^{rx(p)} &= R|P_1/P_{\text{dl}} \\ R|F_2^{rx(p)} &= R|P_2/P_{\text{dl}}.R|\Delta\text{ph}. \end{aligned} \tag{36}$$

From (35) and (36), the results are associated with reporting errors as

$$\begin{aligned} R|F_1^{rx(p)} &= \frac{P_{\text{in1}}}{E_1 * P_{\text{dl}}} \\ R|F_2^{rx(p)} &= \frac{P_{\text{in2}}}{E_2 * P_{\text{dl}}} \\ R|\Delta\text{ph} &= \Delta\text{ph} - \psi. \end{aligned} \tag{37}$$

The measured antenna patterns contain the reporting errors, which are needed to be issued carefully for guaranteeing the test accuracy. Note that (35)–(37) are introduced for the antenna pattern tests and the RSRP reporting errors descriptions. In the rest of this paper, the RSRP reporting errors will be rewritten in the other format for better explanations of the error elimination process.

2) Throughput Test Signals Calculations: For the uth receiver, the real actual antenna patterns are related to the RSRP reads as

$$\begin{bmatrix} F_u^{rx(V)}(\Omega_n^{rx}) * E_u e^{\,j\psi_u} \\ F_u^{rx(H)}(\Omega_n^{rx}) * E_u e^{\,j\psi_u} \end{bmatrix} = \begin{bmatrix} R|F_u^{rx(V)}(\Omega_n^{rx}) \\ R|F_u^{rx(H)}(\Omega_n^{rx}) \end{bmatrix} \tag{38}$$

where $R|F_u^{rx(p)}(\Omega_n^{rx})$ is the measured complex gain based on the reporting system in the polarization p for the uth receiver (within reporting errors); $F_u^{rx(p)}(\Omega_n^{rx})$ is the real actual complex gain in the polarization p for the uth receiver, which is unknown; and E_u and ψ_u are the related amplitude and phase reporting errors (unknown), respectively. Especially, $\psi_j = 0$ while the jth received vector's absolute phase is taken as a reference, since only the relative phase offset is reported. The reporting errors description (38) are same physically, but different in form with (37).

Therefore, according to (16) and (38) the combination of the measured UE antenna patterns and the channel model for 2×2 MIMO test can be described as

$$\begin{aligned} y(t) = \Bigg(\sum_{n=1}^{N} \begin{bmatrix} \begin{bmatrix} R|F_1^{rx(V)}(\Omega_n^{rx}) \\ R|F_1^{rx(H)}(\Omega_n^{rx}) \end{bmatrix}^T & 0 \\ 0 & \begin{bmatrix} R|F_2^{rx(V)}(\Omega_n^{rx}) \\ R|F_2^{rx(H)}(\Omega_n^{rx}) \end{bmatrix}^T \end{bmatrix} \\ \cdot \begin{bmatrix} \Theta_{n,1,1} & \Theta_{n,1,2} \\ \Theta_{n,2,1} & \Theta_{n,2,2} \end{bmatrix} \Bigg) * x(t) \end{aligned} \tag{39}$$

which is also the real throughput test signal calculation.

From (38) and (39), the throughput test signals become

$$\begin{aligned} y(t) = \Bigg(\sum_{n=1}^{N} \begin{bmatrix} E_1 e^{\,j\psi_1} & 0 \\ 0 & E_2 e^{\,j\psi_2} \end{bmatrix} \\ \cdot \begin{bmatrix} \begin{bmatrix} F_1^{rx(V)}(\Omega_n^{rx}) \\ F_1^{rx(H)}(\Omega_n^{rx}) \end{bmatrix}^T & 0 \\ 0 & \begin{bmatrix} F_2^{rx(V)}(\Omega_n^{rx}) \\ F_2^{rx(H)}(\Omega_n^{rx}) \end{bmatrix}^T \end{bmatrix} \\ \cdot \begin{bmatrix} \Theta_{n,1,1} & \Theta_{n,1,2} \\ \Theta_{n,2,1} & \Theta_{n,2,2} \end{bmatrix} \Bigg) * x(t). \end{aligned} \tag{40}$$

Authorized licensed use limited to: HUNAN UNIVERSITY. Downloaded on March 04,2021 at 08:41:10 UTC from IEEE Xplore. Restrictions apply.

Since the reporting error matrix $\begin{bmatrix} E_1 e^{j\psi_1} & 0 \\ 0 & E_2 e^{j\psi_2} \end{bmatrix}$ is independent of the parameter n (the number of arrival clusters defined in the channel model), (40) further becomes

$$y(t) = \begin{bmatrix} E_1 e^{j\psi_1} & 0 \\ 0 & E_2 e^{j\psi_2} \end{bmatrix} \cdot \left(\sum_{n=1}^{N} \begin{bmatrix} \begin{bmatrix} F_1^{rx(V)}(\Omega_n^{rx}) \\ F_1^{rx(H)}(\Omega_n^{rx}) \end{bmatrix}^T & 0 \\ 0 & \begin{bmatrix} F_2^{rx(V)}(\Omega_n^{rx}) \\ F_2^{rx(H)}(\Omega_n^{rx}) \end{bmatrix}^T \end{bmatrix} \cdot \begin{bmatrix} \Theta_{n,1,1} & \Theta_{n,1,2} \\ \Theta_{n,2,1} & \Theta_{n,2,2} \end{bmatrix} \right) * x(t). \quad (41)$$

Equation (41) indicates the real calculated throughput test signal vector, including the reporting errors.

3) Received Signals at RF Receiver Inputs: The throughput test signals are delivered passing the inverse matrix, propagation matrix, and then fed into the receivers. So the function of the throughput test signals $y(t)$ with the actual received signals at the MIMO DUT receiver inputs $R(t)$ is

$$R(t) = P \cdot M' * y(t) \quad (42)$$

where P is the propagation matrix; M' is the practical loaded inverse matrix solved in Section III-B, as shown in (31)–(34).

It is worth noting that the inverse matrix solving (30)–(34) are based on the measured DUT antenna patterns (consisting the RSRP reporting errors). For the uth receiver, the measured antenna patterns are recorded as $\begin{bmatrix} R|F_u^{rx(V)}(\Omega_n^{rx}) \\ R|F_u^{rx(H)}(\Omega_n^{rx}) \end{bmatrix}$ in this part. Therefore, we can rewrite (31) as (43), shown at the bottom of the next page. Substituting (38) into (43), we can have (44), shown at the bottom of the next page, to illustrate the real applied inverse matrix M', where A is the normalization parameter. Combining (41), (42), and (44), the real actual received signal vector at DUT receiver input $R(t)$ is re-expressed as (45), shown at the bottom of the next page. Furthermore, the propagation matrix is

$$P^{-1} = e^{-j\varphi_{1V}} * P''^{-1}. \quad (46)$$

Thus, the real received signal vector is expressed as (47), shown at the bottom of the next page, where $(e^{j\varphi_{1V}}/A)$ is the virtual cables' path loss and phase offset. And finally, the errors $\begin{bmatrix} E_1 e^{j\psi_1} & 0 \\ 0 & E_2 e^{j\psi_2} \end{bmatrix}$ are eliminated in signal $R(t)$, which indicates that no reporting errors are fed into the receiver inputs in the final throughput test process.

In summary, the RSRP reporting errors are eliminated during the entire RTS test process. Besides its advantages on improving the RTS test accuracy, no more extra test steps are required.

In fact, experiments were carried out on a MIMO device with errors of more than ±1.3 dB for power evaluations at both receivers, and an error of more than ±7.5° for the phase evaluation [29]. Results showed that without issuing the reporting errors, the impact on the final throughput test may be larger than ±1.6 dB. Hence, the elimination techniques are available to reduce the RTS MIMO OTA test uncertainties.

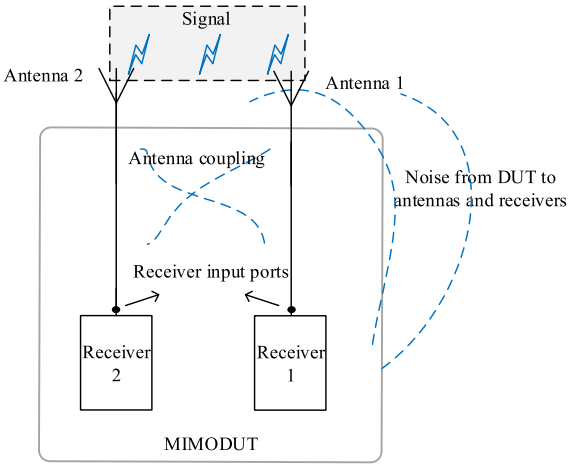

Fig. 17. Typical 2 × 2 MIMO system diagram.

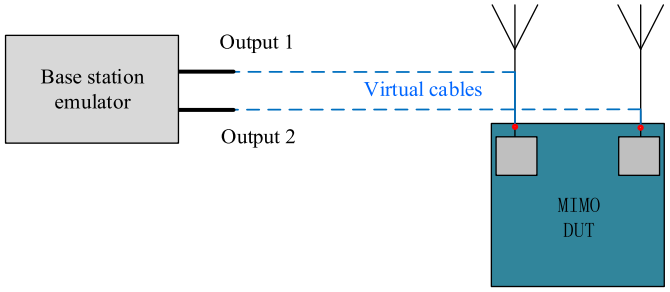

Fig. 18. Simplified system for the two radiated sensitivity measurements.

Additionally, (47) is the complete expression of the RTS MIMO OTA test method. It is the first time that the entire RTS process is expressed mathematically.

D. MIMO Device Troubleshooting Based on the RTS Method

Throughput is the only FoM for MIMO OTA performance evaluations, and for DUT network certifications. For a MIMO device, both MPAC and RTS can create channel models and provide the final throughput test results and then help to distinguish between the qualified and unqualified devices. However, only the RTS method could help with MIMO device troubleshooting and diagnosis. Generally, for a MIMO system, the antennas and receivers are designed by different departments. The DUT integrated OTA performance could differ from the conducted antenna performance plus the conducted receiver performance, so MIMO system diagnosis could locate the problem and greatly raise the efficiency of R&D.

A typical 2 × 2 MIMO system is illustrated in Fig. 17. The self-interference (mainly caused by the power block and the digital modules inside), the coupling noise, and the mismatch may cause large sensitivity degradation. The RTS-based diagnosis technique is built on two facts. First, the RTS method could not only provide the throughput results, but also the antenna patterns. Those are useful for antenna analysis, such as the antenna envelope correlation coefficient, the active efficiency, the antenna imbalance, etc. Second, with the inverse matrix loaded, the instrument outputs are linked to the receiver inputs directly (via virtual cables), as simplified in Fig. 18.

Authorized licensed use limited to: HUNAN UNIVERSITY. Downloaded on March 04,2021 at 08:41:10 UTC from IEEE Xplore. Restrictions apply.

Then, each receiver can be diagnosed separately, such as the radiated sensitivity test and the desensitization test. Different from the conducted sensitivity, radiated sensitivity could reflect the RF receiver performance under the integrated state (real working state without conductive cables). In other words, the self-interference shown in Fig. 17 is considered in the radiated sensitivity measurement.

E. Recent Progress of the RTS Method

RTS and MPAC are both recommended methods in the 3GPP technical report 37.977 since 2014 [21]. Both of them are also the only two standard methods in the latest 3GPP TS 37.544 in 2018 (the global standard for specifying the wireless OTA measurement) [18]. The MPAC method is the only standard technique in the CTIA MIMO OTA test plan [15]. The RTS standardization process in the CTIA is in progress.

From April 2017 to July 2017, the 3GPP held a harmonization comparison measurement for the MIMO OTA test standardizations. Three methods were introduced: the MPAC method, which was already the standard method since 2015; the RTS method, and the reverberation chamber plus channel emulator (RC + CE) method.

The RC + CE method was not discussed in this paper for two reasons. First, the RC + CE method could not create the standard channel models defined in the 3GPP white papers. Therefore, the theory foundations are not widely recognized. Second, the RC + CE method failed to pass this harmonization comparison measurement hosted by the 3GPP, since there is no comparability between the results provide by the RC+CE method and the other two methods [31], [32]. Thus, only the comparisons between the RTS and MPAC are introduced as below.

1) Test Set-Ups: The harmonization measurements were carried out in the China Academy of Telecommunication Research (CATR), where both certified MPAC and RTS test systems are provided. For the 2 × 2 RTS MIMO OTA test, a SISO chamber with a horn antenna was used. For the 2 × 2 MPAC MIMO OTA test, a chamber with eight horn antennas surrounding environment was used. There are totally eight DUTs, four test bands, three test positions, and one channel model, resulting in 96 groups of throughput test results for the two methods. The detailed set-ups for the DUT and instruments can be shown in Table III and referred to in the 3GPP report [31].

TABLE III
MEASUREMENT PARAMETERS FOR HARMONIZATION MEASUREMENTS

Parameters	Values
DUTs	Eight 2×2 MIMO supported devices from different companies were used as DUTs.
Test frequencies	Band 3, Band 5, Band 7, Band 13
DUT positions	P 45, L 45, P 90
Test channel model	The spatial channel model extension Umi

TABLE IV
THROUGHPUT RESULT COMPARISONS BETWEEN THE MPAC AND THE RTS

Band	Downlink frequency (MHz)	Measurement result difference (dB)
13	751.0	0.54
5	881.5	0.50
3	1842.5	0.60
7	2655.0	0.92

2) Results and Accepted Proposals: Totally 96 groups of throughput result comparisons were achieved between the MPAC and RTS, which are listed in Table IV. All differences are within 0.92 dB [31], [32]. Based on the measurement results, several conclusions were proposed in the proposals, where one recognized and accepted recommendation is: "For the FDD bands tested in the MPAC/RTS harmonization, the harmonization cost varies between 0.5 and 0.92 dB. The

$$P'' = \begin{bmatrix} G_{\mathrm{PL}} * G_m^V * R|F_1^{rx(V)}\left(\Omega_n^{rx}\right) & G_{\mathrm{PL}} * G_m^H * R|F_1^{rx(H)}\left(\Omega_n^{rx}\right) * e^{j\delta} \\ G_{\mathrm{PL}} * G_m^V * R|F_2^{rx(V)}\left(\Omega_n^{rx}\right) * e^{j\alpha} & G_{\mathrm{PL}} * G_m^H * R|F_2^{rx(H)}\left(\Omega_n^{rx}\right) * e^{j(\beta+\delta)} \end{bmatrix} \tag{43}$$

$$M' = \frac{1}{A} * \left(\begin{bmatrix} E_1 e^{j\psi_1} & 0 \\ 0 & E_2 e^{j\psi_2} \end{bmatrix} \cdot \begin{bmatrix} G_{\mathrm{PL}} * G_m^V * F_1^{rx(V)}\left(\Omega_n^{rx}\right) & G_{\mathrm{PL}} * G_m^H * F_1^{rx(H)}\left(\Omega_n^{rx}\right) * e^{j\delta} \\ G_{\mathrm{PL}} * G_m^V * F_2^{rx(V)}\left(\Omega_n^{rx}\right) * e^{j\alpha} & G_{\mathrm{PL}} * G_m^H * F_2^{rx(H)}\left(\Omega_n^{rx}\right) * e^{j(\beta+\delta)} \end{bmatrix} \right)^{-1} \tag{44}$$

$$R(t) = \frac{P}{A} * \begin{bmatrix} G_{PL} * G_m^V * F_1^{rx(V)}\left(\Omega_n^{rx}\right) & G_{PL} * G_m^H * F_1^{rx(H)}\left(\Omega_n^{rx}\right) * e^{j\delta} \\ G_{PL} * G_m^V * F_2^{rx(V)}\left(\Omega_n^{rx}\right) * e^{j\alpha} & G_{PL} * G_m^H * F_2^{rx(H)}\left(\Omega_n^{rx}\right) * e^{j(\beta+\delta)} \end{bmatrix}^{-1} \cdot \left(\sum_{n=1}^{N} \begin{bmatrix} \begin{bmatrix} F_1^{rx(V)}\left(\Omega_n^{rx}\right) \\ F_1^{rx(H)}\left(\Omega_n^{rx}\right) \end{bmatrix}^T & 0 \\ 0 & \begin{bmatrix} F_2^{rx(V)}\left(\Omega_n^{rx}\right) \\ F_2^{rx(H)}\left(\Omega_n^{rx}\right) \end{bmatrix}^T \end{bmatrix} \cdot \begin{bmatrix} \Theta_{n,1,1} & \Theta_{n,1,2} \\ \Theta_{n,2,1} & \Theta_{n,2,2} \end{bmatrix} \right) * x(t) \tag{45}$$

$$R(t) = \frac{e^{j\varphi_{1V}}}{A} * \left(\sum_{n=1}^{N} \begin{bmatrix} \begin{bmatrix} F_1^{rx(V)}\left(\Omega_n^{rx}\right) \\ F_1^{rx(H)}\left(\Omega_n^{rx}\right) \end{bmatrix}^T & 0 \\ 0 & \begin{bmatrix} F_2^{rx(V)}\left(\Omega_n^{rx}\right) \\ F_2^{rx(H)}\left(\Omega_n^{rx}\right) \end{bmatrix}^T \end{bmatrix} \cdot \begin{bmatrix} \Theta_{n,1,1} & \Theta_{n,1,2} \\ \Theta_{n,2,1} & \Theta_{n,2,2} \end{bmatrix} \right) * x(t). \tag{47}$$

Authorized licensed use limited to: HUNAN UNIVERSITY. Downloaded on March 04,2021 at 08:41:10 UTC from IEEE Xplore. Restrictions apply.

harmonization cost is within the harmonization target for all bands and, therefore, harmonization between MPAC and RTS for bands 13, 5, 3, and 7 can be confirmed." Further, the comparisons on TDD bands were presented, the differences are within 1 dB [18]. Based on the comparisons, the RTS was accepted to be a standard MIMO OTA test method and added into the 3GPP TS 37.544 v14.5.0, 2018 [18].

In addition, one more contribution was proposed in this meeting [24], where comparison measurements were carried out among different MPAC systems (not including the system in the CATR) under the same configurations. Experiments showed that the maximal result difference between those MPAC chambers within the same set-ups and same DUTs is up to 7.31 dB, which is much larger than the defined MPAC test uncertainties. This indicates that although the MPAC method is correct in theory foundations, it is difficult to implement accurately. For the MPAC method, every element and process for the complex system (including multiple antennas, multichannel simulator, etc.) is required to be handled accurately. Besides, only in the condition that all elements and processes are calibrated and executed accurately, RTS and MPAC will have the same results.

IV. Conclusion

Directly adopting the 3GPP and CTIA standard OTA measurement for IoT wireless performance evaluations could cause a high cost, a long test period, and a great test uncertainty. It is the major challenge that impedes OTA test techniques being popularized in the IoT industry. For meeting the ubiquitous and massive test requirements of IoT, this paper provides several solutions to ensure that the IoT OTA measurement could be conducted in accurate, fast, and cost-efficient approaches.

For the single-antenna configured devices, three techniques are introduced for speeding up its SISO OTA performance measurement and improving the test accuracy. The provided test system is suitable for office buildings. Based on that, the test time is reduced by 4–12 times.

For the MIMO devices, the RTS method was demonstrated in both theory foundations and recent progress. For the RTS method, SISO chamber is suitable for MIMO OTA test with software up-gradations. The channel models are calculated through instruments mathematically with the antenna pattern measurement errors eliminated. Much simpler hardware and clear theory deductions make the RTS a reliable and low measurement uncertainty MIMO OTA test solution, which was also proven in the last section of this paper.

The proposed solutions could almost cover all types of IoT wireless technologies. Besides, MIMO techniques are the basic of 4G LTE and 5G beam forming communications. As a reliable, cost-efficient MIMO OTA measurement solution, the progress in this paper is a summary for the RTS method in 4G and introduction in 5G communications.

References

[1] D. B. Rawat, T. White, M. S. Parwez, C. Bajracharya, and M. Song, "Evaluating secrecy outage of physical layer security in large-scale MIMO wireless communications for cyber-physical systems," *IEEE Internet Things J.*, vol. 4, no. 6, pp. 1987–1993, Dec. 2017.

[2] H. Zhou *et al.*, "Toward 5G spectrum sharing for immersive-experience-driven vehicular communications," *IEEE Wireless Commun.*, vol. 24, no. 6, pp. 30–37, Dec. 2017.

[3] Y. Jing, H. Kong, and M. Rumney, "MIMO OTA test for a mobile station performance evaluation," *IEEE Instrum. Meas. Mag.*, vol. 19, no. 3, pp. 43–50, Jun. 2016.

[4] H. Ko, G. Lee, D. Suh, S. Pack, and X. Shen, "An optimized and distributed data packet forwarding scheme in LTE/LTE-A networks," *IEEE Trans. Veh. Technol.*, vol. 66, no. 5, pp. 3462–3473, May 2016.

[5] Y. Jing, Z. Wen, H. Kong, S. Duffy, and M. Rumney, "Two-stage over the air (OTA) test method for MIMO device performance evaluation," in *Proc. IEEE Int. Symp. Antennas Propag.*, 2011, pp. 71–74.

[6] Y. Qi *et al.*, "5G over-the-air measurement challenges: Overview," *IEEE Trans. Electromagn. Compat.*, vol. 59, no. 6, pp. 1661–1670, Dec. 2017.

[7] Y. Qi and W. Yu, "Unified antenna temperature," *IEEE Trans. Electromagn. Compat.*, vol. 58, no. 5, pp. 1425–1431, Oct. 2016.

[8] P. Shen, Y. Qi, W. Yu, F. Li, and J. Fan, "Fast and accurate TIS testing method for wireless user equipment with RSS reporting," *IEEE Trans. Electromagn. Compat.*, vol. 58, no. 3, pp. 887–895, Jun. 2016.

[9] P. Shen *et al.*, "A decomposition method for MIMO OTA performance evaluation," *IEEE Trans. Veh. Technol.*, to be published, doi: 10.1109/TVT.2018.2839726.

[10] L. Hong and A. G. Armada "Bit error rate performance of MIMO MMSE receivers in correlated Rayleigh flat-fading channels," *IEEE Trans. Veh. Technol.*, vol. 60, no. 1, pp. 313–317, Jan. 2010.

[11] "V14.5.0," 3GPP, Sophia Antipolis, France, Rep. 37.977, 2017. [Online]. Available: http://www.3gpp.org

[12] *Test Plan for Mobile Station Over the Air Performance, Revision 3.3.5*, CTIA, Washington, DC, USA, Jul. 2016.

[13] General Test Systems Inc., "Method and device for testing performance of wireless terminal," U.S. Patent 14 441 061, Feb. 22, 2017. [Online]. Available: http://appft1.uspto.gov/netacgi/nph-Parser?Sect1=PTO1&Sect2=HITOFF&d=PG01&p=1&u=/netahtml/PTO/srchnum.html&r=1&f=G&l=50&s1=20150280844.PGNR

[14] J. T. Wang, "Throughput-based switching between diversity and multiplexing in MIMO systems with cochannel interference," *IEEE Trans. Veh. Technol.*, vol. 58, no. 7, pp. 3850–3855, Sep. 2009.

[15] *Test Plan for 2 × 2 Downlink MIMO and Transmit Diversity Over-the-Air Performance, Revision 1.1*, CTIA, Washington, DC, USA, Aug. 2016.

[16] Y. Qi, P. Jarmuszewski, Q. Zhou, M. Certain, and J. Chen, "An efficient TIS measurement technique based on RSSI for wireless mobile stations," *IEEE Trans. Instrum. Meas.*, vol. 59, no. 9, pp. 2414–2419, Sep. 2010.

[17] J. Anderson, T. Aulin, and C. Sundberg, *Digital Phase Modulation*. New York, NY, USA: Plenum, 1986.

[18] *V14.6.0*, 3GPP Standard TS 37.544, 2018. [Online]. Available: http://www.3gpp.org

[19] W. Liang, Y. Qi, and Y.-C. Jiao, "A novel small director array for slot loop antenna for LTE application," *IEEE Antennas Wireless Propag. Lett.*, vol. 12, pp. 1110–1113, 2013.

[20] W. Fan, P. Kyösti, J. Ø. Nielsen, and G. F. Pedersen, "Wideband MIMO channel capacity analysis in multiprobe anechoic chamber setups," *IEEE Trans. Veh. Technol.*, vol. 65, no. 5, pp. 2861–2871, May 2016.

[21] W. Yu, Y. Qi, K. Liu, Y. Xu, and J. Fan, "Radiated two-stage method for LTE MIMO user equipment performance evaluation," *IEEE Trans. Electromagn. Compat.*, vol. 56, no. 6, pp. 1691–1696, Dec. 2014.

[22] W. Xu *et al.*, "Internet of Vehicles in big data era," *IEEE/CAA J. Automatica Sinica*, vol. 5, no. 1, pp. 19–35, Jan. 2018.

[23] D. Zhang, Z. Zhou, S. Mumtaz, J. Rodriguez, and T. Sato, "One integrated energy efficiency proposal for 5G IoT communications," *IEEE Internet Things J.*, vol. 3, no. 6, pp. 1346–1354, Dec. 2016.

[24] *CTIA & CCSA Combined Comparison Test Plan and Proposal*, document 3GPP RAN4 #83, MOSG170406, Huawei, Shenzhen, China, Apr. 2017.

[25] "Measurements of radiated performance for MIMO and multi-antenna reception for HSPA and LTE terminals, v11.0.0," 3GPP, Sophia Antipolis, France, Rep. 37.976, 2012.

[26] J. Cai, X. Shen, J. W. Mark, H. Liu, and T. D. Todd, "Semiblind channel estimation for pulse-based ultra-wideband wireless communication systems," *IEEE Trans. Veh. Technol.*, vol. 55, no. 1, pp. 95–103, Jan. 2016.

[27] H. Kong, Z. Wen, Y. Jing, and M. Yau, "A compact millimeter wave (mmWave) mid-field over the air (OTA) RF performance test system for 5G massive MIMO devices," in *Proc. IEEE MTT-S Int. Wireless Symp. (IWS)*, 2018, pp. 1–4.

Authorized licensed use limited to: HUNAN UNIVERSITY. Downloaded on March 04,2021 at 08:41:10 UTC from IEEE Xplore. Restrictions apply.

[28] P. Shen, Y. Qi, W. Yu, and F. Li, "Inverse matrix auto-search technique for the RTS MIMO OTA test—Part 1: Theory," *IEEE Trans. Electromagn. Compat.*, vol. 59, no. 6, pp. 1716–1723, Dec. 2017.
[29] P. Shen, Y. Qi, W. Yu, and F. Li, "Eliminating RSARP reporting errors in the RTS method for MIMO OTA test," *IEEE Trans. Electromagn. Compat.*, vol. 59, no. 6, pp. 1708–1715, Dec. 2017.
[30] P. Shen, Y. Qi, W. Yu, and F. Li, "Inverse matrix auto-search technique for the RTS MIMO OTA test—Part II: Validations," *IEEE Trans. Electromagn. Compat.*, vol. 60, no. 5, pp. 1288–1295, Oct. 2018.
[31] *Analysis of Harmonization Results*, document 3GPP RAN4 #83, R4-1704578, Rohde & Schwarz, Munich, Germany, May 2017.
[32] *Harmonization Analysis*, document 3GPP RAN4 #83, R4-1704661, CATR, Intel Corporat., Santa Clara, CA, USA, May 2017.
[33] *General Test Systems Inc.* [Online]. Available: http://www.trilsolutions.com/english.php/rayzone
[34] M.-T. Dao, V.-A. Nguyen, Y.-T. Im, S.-O. Park, and G. Yoon, "3D polarized channel modeling and performance comparison of MIMO antenna configurations with different polarizations," *IEEE Trans. Antennas Propag.*, vol. 59, no. 7, pp. 2672–2682, Jul. 2011.
[35] A. F. Molisch, "A generic model for MIMO wireless propagation channels," in *Proc. IEEE ICC*, vol. 1, May 2002, pp. 277–282.
[36] M. Rumney, H. Kong, Y. Jing, Z. Zhang, and P. Shen, "Recent advances in the radiated two-stage MIMO OTA test method and its value for antenna design optimization," in *Proc. 10th Eur. Conf. Antennas Propag. (EuCAP)*, 2016, pp. 1–5.

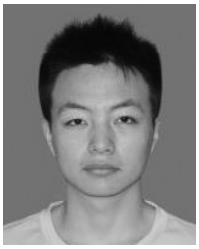

Penghui Shen (S'15) received the B.S. and M.S. degrees in electronic information and technology from Hunan University, Changsha, China, in 2013 and 2016, respectively, where he is currently pursuing the Ph.D. degree in electronics.

His current research interests include single-input single-output, multi-input multioutput, and 5G array measurements for wireless devices, EMC, and antenna design.

Yihong Qi (M'92–SM'11) received the B.S. degree in electronics from the National University of Defense Technologies, Changsha, China, in 1982, the M.S. degree in electronics from the Chinese Academy of Space Technology, Beijing, China, in 1985, and the Ph.D. degree from Xidian University, Xi'an, China, in 1989.

From 1989 to 1993, he was a Post-Doctoral Fellow and then an Associate Professor with Southeast University, Nanjing, China. From 1993 to 1995, he was a Post-Doctoral Researcher with McMaster University, Hamilton, ON, Canada. From 1995 to 2010, he was with Research in Motion, Blackberry, Waterloo, ON, Canada, where he was the Director of Advanced Electromagnetic Research. He is currently the President and the Chief Scientist with General Test Systems, Inc., Shenzhen, China. He founded DBJay in 2011, and he is the CTO of ENICE. He is also an Adjunct Professor with the EMC Laboratory, Missouri University of Science and Technology, Rolla, MO, USA, and Hunan University, Changsha. He holds over 270 issued and pending patents.

Dr. Qi was a recipient of the IEEE EMC Society Technical Achievement Award in 2017. He was a Distinguished Lecturer of the IEEE EMC Society in 2014 and 2015 and serves as the Chairman of IEEE EMC TC-12. He has been a Fellow of the Canadian Academy of Engineering since 2018.

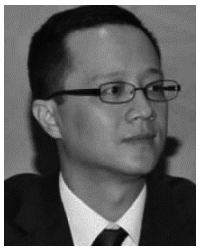

Wei Yu (M'13) received the B.S. degree in electrical engineering from Xi'an Jiaotong University, Xi'an, China, in 1991, the M.S. degree in electrical engineering from the China Academy of Space Technology, Beijing, China, in 1994, and the Ph.D. degree in electrical engineering from Xidian University, Xi'an, in 2000.

From 2001 to 2003, he was a Post-Doctoral Fellow with the University of Waterloo, Waterloo, ON, Canada. He was the CTO of Sunway Communications, Ltd., Shenzhen, China, from 2008 to 2012. He founded Antenovation Electronics, Inc., in 2004, and co-founded General Test Systems Inc., Shenzhen, in 2012. He is currently a COO with DBJ Technologies, Zhuhai, China. He holds 91 issued and pending patents. His current research interests include signal processing and mobile device test systems.

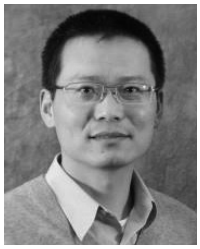

Jun Fan (S'97–M'00–SM'06–F'16) received the B.S. and M.S. degrees in electrical engineering from Tsinghua University, Beijing, China, in 1994 and 1997, respectively, and the Ph.D. degree in electrical engineering from the University of Missouri, Rolla, MO, USA, in 2000.

From 2000 to 2007, he was with the NCR Corporation, San Diego, CA, USA, as a Consultant Engineer. In 2007, he joined the Missouri University of Science and Technology (formerly the University of Missouri), where he is currently an Associate Professor with the Missouri S&T EMC Laboratory. His current research interests include signal integrity and EMI designs in high-speed digital systems, dc power-bus modeling, intersystem EMI and radio frequency interference, PCB noise reduction, differential signaling, and cable/connector designs.

Dr. Fan was a recipient of the IEEE EMC Society Technical Achievement Award in 2009. He is an Associate Editor of *EMC Magazine* and the IEEE TRANSACTIONS ON ELECTROMAGNETIC COMPATIBILITY. He was the Chair of the IEEE EMC Society TC-9 Computational Electromagnetics Committee from 2006 to 2008 and a Distinguished Lecturer of the IEEE EMC Society in 2007 and 2008. He is currently the Vice Chair of the Technical Advisory Committee of the IEEE EMC Society.

Fuhai Li (M'16) received the B.S. and M.S. degrees in instrument science and technology from Hunan University, Changsha, China, in 1982 and 1988, respectively.

He was a Professor with Hunan University. He has authored or co-authored over 22 papers in the national core journals and involved the compiling of university teaching materials.

Mr. Li was a recipient of several science and technology progress awards. His students have been the recipients of many awards in numerous varied national competitions under his leadership.

Authorized licensed use limited to: HUNAN UNIVERSITY. Downloaded on March 04,2021 at 08:41:10 UTC from IEEE Xplore. Restrictions apply.